Proceedings World Geothermal Congress 2005
Antalya, Turkey, 24-29 April 2005

Geothermal Heat and Abandoned Gas Reservoirs in the Netherlands

Geert K. Brouwer, Ad Lokhorst and Bogdan Orlic

Princetonlaan 6, P.O. Box 80015, 3508 TA Utrecht, the Netherlands

g.brouwer@nitg.tno.nl

Keywords: sustainable, gas reservoir, modelling

ABSTRACT

Sustainable energy in the Netherlands is delivered with success from shallow sub-surface systems, but from depths greater than a few hundreds of metres this is still uncertain. A serious effort to exploit thermal energy from depths where temperatures are sufficiently high for energy companies (>75 ^{o}C) was performed at the Vinex (new town extension) location Barendrecht near Rotterdam. A gas field to be abandoned in a few years, could serve as a recipient of the water produced from a selected "hot spot" from the IJsselmonde sandstone at a depth of nearly 2000 m with temperatures of 75-80 ^{o}C. A conventional gas reservoir study including interpretation of 3-D seismic data (horizon determination), facies modelling of a complex fluvial-marine environment, petrophysical interpretation of logs of approximately ten wells, hydrochemistry, drilling engineering, reservoir modelling including thermal modelling and geomechanical modelling was performed to delineate the hydraulic, thermal and mechanical behaviour of the reservoir. Probabilistic geological models, generated with state of the art modeling software, were imported in an industry standard black oil simulator. The distance between producer and injector was carefully selected to prevent thermal breakthrough, while maximising the temperature of the produced water. Meanwhile the amount of produced water should fulfil a minimum requirement of 3.2 MW thermal energy with acceptable pressure differences in the wells.

1. INTRODUCTION

Sustainable energy in the Netherlands is delivered with success from shallow sub-surface (mainly heat/cold storage) systems, but from depths greater than a few hundreds of metres this is still not the case. However, since the Kyoto agreement, renewed interest in the low enthalpy geothermal energy emerges in The Netherlands, resulting in feasibility studies in areas where promising geological conditions are met in combination with the possibility of the development of district heating systems in new suburban areas (so-called VINEX locations) or where the replacement of older fossil fuel based heating facilities is necessary due to their economic lifetime.

A serious effort to exploit thermal energy from depths where temperatures are sufficiently high for energy companies (>75 ^{o}C) was performed at a VINEX location near Barendrecht (Rotterdam area). A gas field to be abandoned in a few years, could serve as the recipient of the water produced from the IJsselmonde sandstone at a depth of nearly 2000 m with temperatures of 75-80 ^{o}C.

2. GEOLOGICAL SETTING

The main target of the Barendrecht feasibility study are the Lower Cretaceous IJsselmonde sandstone's, deposited at the southern limbs of the West-Netherlands Basin. The IJsselmonde sandstone form a part of a stepwise north to south deposited series of transgressive marine sands and coastal barriers. These sands form the main reservoirs of the West Netherlands Oil and Gas province (Racero-Baena and Drake, 1996). In the study area a producing gas field is present in a small anticlinal structure. Based on log data the lower part of the sequence consists of a 15 to 20 m thick transgressive coastal barrier sandstone, followed by a 30 to 40 m thick fluvial sequence of clay and sandstone (50%) and on top of that an 80 m thick claystone sequence with some minor intercalation's of sandstone's. Log correlations between the wells clearly show the heterogeneous character of the fluvial part of the aquifer (De Vault and Jeremiah, 2002).

In order to build a proper porosity and permeability model for the Eclipse simulation a 3-D grid model, based on 3-D seismic data, petrophysical data and the geological assumptions on the sedimentary character of the IJsselmonde sandstone was generated. Based on the dual character of the IJsselmonde sandstone, the fluvial part of the sequence was given a facies code based on the stochastic fluvial facies routine of the Petrel software. Figure 1 shows a facies realisation of the fluvial part of the IJsselmonde sandstone.

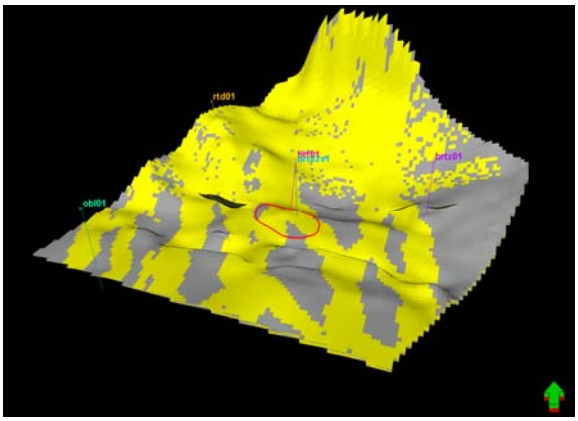

Figure 1: A facies realisation of the fluvial part of the IJsselmonde sandstone displaying (yellow) the distribution of sand-rich parts (>50%) of the deposits.

Porosity and permeability were generated, by Sequential Gaussian Simulation. The resulting 3D grid was input for the Eclipse modelling. Figure 2 shows one of the porosity realisations of the basal transgressive sandsheet.

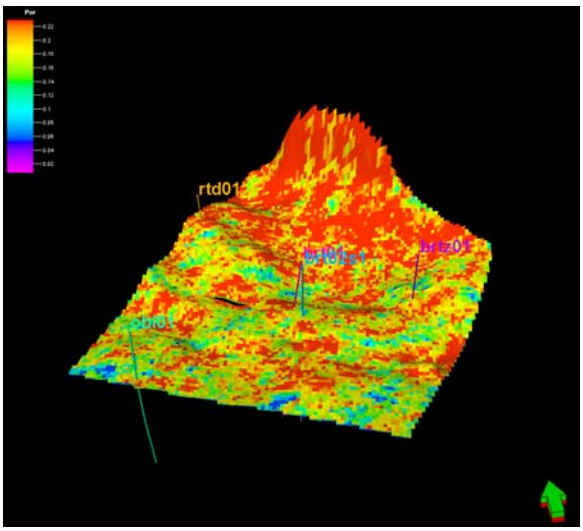

Figure 2: A porosity realisation of the basal transgressive IJsselmonde sandstone. The porosity range is from 5% (dark-blue) to 23% (red).

The porosity values have been derived from the available density- and neutron logs.

Porosity and net sandstone thickness derived from the logs of the wells in the vicinity of the Barendrecht vary from about 18 to 21%, whereas wells further away from Barendrecht show porosities from about 15%. Net sand thickness varies from 22 up to 36 meter.

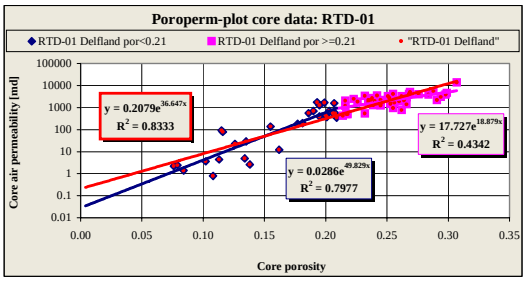

Figure 3: Poroperm plot of the Delfland sandstone in well RTD-01.

In order to calculate the permeability a poroperm relationship is based on available core data of the (comparable) Delfland sandstone (which is also present in the area) of well BRT-1. Figure 3 shows the poroperm relationship based on this analysis. Two linear relationships have been distinguished, based on the porosity value (i.e. 21%).

Based on this analysis the permeabilities of the sandstones are estimated to vary from 180 up to 450 mD in the direct vicinity of the Barendrecht location and lower values further away from the area, indicating the possibility of strong variation of the permeability, probably due to the strong heterogeneous character of the fluvial sandstones.

3. THE DYNAMIC HEAT AND FLOW MODEL

The Eclipse blackoil simulator was used to model the thermal transport. The thermal transport was estimated with the black oil simulator Eclipse-100 (Eclipse-100 Manual, Technical description). With this model the temperature of the injection water is defined. With a thermal gradient the initial temperature distribution is calculated in Eclipse. This thermal gradient was estimated from temperature measurements in surrounding wells of the gas field.

Thanks to the presence of a temperature gradient survey at a depth of about 2500 – 3000 m (well BRTZ-01), combined with log header data of nearby wells, it was possible to estimate the temperature-depth relationship in the area quite accurately (Figure 4) resulting in the following T-D relationship:

$$T=0.0293*D+20.381 \quad (1)$$

where T, D are temperature and depth, respectively.

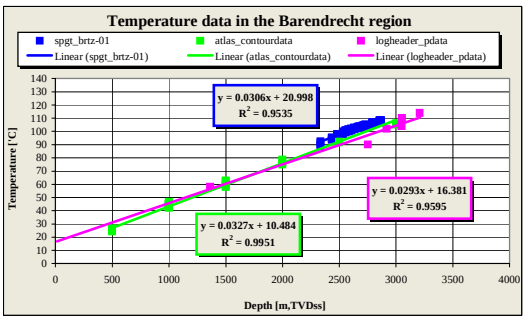

Figure 4: Temperature-depth relationship.

The temperature variation of the target formation is given in Figure 5.

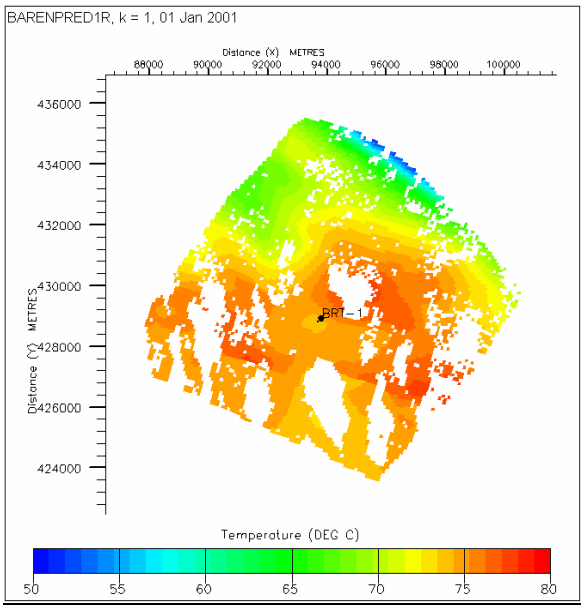

Figure 5: Temperature distribution top reservoir for injection/production.

Along the northeastern boundary the low temperature is due to the shallow depth of the IJsselmonde sands. BRT-1 is the existing production well. The white areas are the clayey parts of the reservoir.

Conductive transport is possible through adjacent layers of the gas reservoir. Because conductive transport is a much slower process than convective heat transport, these heat losses are initially neglected.

Table 1: Geothermal parameters.

Rock	
Heat capacity	1.0 kJ/kg/^{o}C
Specific heat	0.9 kJ/kg.^{o}C
Density	2900 kg/m^{3}
Viscosity	temperature dependent
Formation water	
Heat capacity	4.184 kJ/kg/^{o}C
Specific heat	4.22 kJ/kg.^{o}C
Density	1015 kg/m^{3}
Thermal conductivity	2.5-5.0 W/m/^{o}C (Somerton, 1992)

3.1 The numerical model

The 3D numerical grid for Eclipse has 10 layers. The number of cells in de x-direction and y-direction are the same as in the geological Petrel model respectively 122 and 108. So no up-scaling was needed. The upper seven layers are sandy fluviatile sediments. The lower three layers are more homogeneous and represent the basal transgressive sandsheet layers. All layers have a trend in thickness: layer thickness increases from 5 m in the south eastern part of the model area to 15 m in the north western part.

Calibration of the field: 55% model

To get a reliable model measured pressures are compared with calculated pressures. The oil gas field was modelled during the production phase. PVT data are included in the model as well as relative permeability curves. The reservoir was initialised hydrostatically with an oil water contact at a depth of 1839 m and a gas oil contact at a depth of 1832 m. Gas initially in place (GIIP) and oil initially in place (STOIP) were compared with literature figures (Table 2).

Table 2: STOIP and GIIP according to Eclipse model and former gas field study.

	TNO-NITG	Gas field analysis
GIIP (10^{9} Sm^{3})	0.23	0.34
STOIP (10^{6} Sm^{3})	0.53	0.57

The relatively large difference in GIIP is due to less volume in the upper part of the reservoir. The gas production data of BRT-1 and BRT-2 are modelled on a monthly basis. Because only tubing head pressures (THP) have been measured during production, calculated bottom hole pressures (BHP) were converted to THP with lift curves (well model). The gas production (green line), calculated BHP (red line) and THP (symbol: star) are shown in Figure 6a (BRT-1) and Figure 6b (BRT-2). The measured THP are approx. 140 bar and are in agreement with calculated THP's.

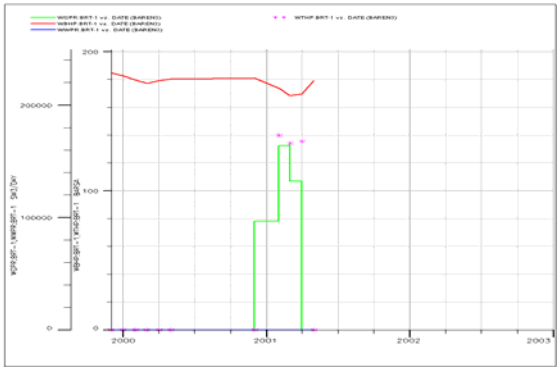

Figure 6a: Gas production, calculated BHP and THP of well BRT-1.

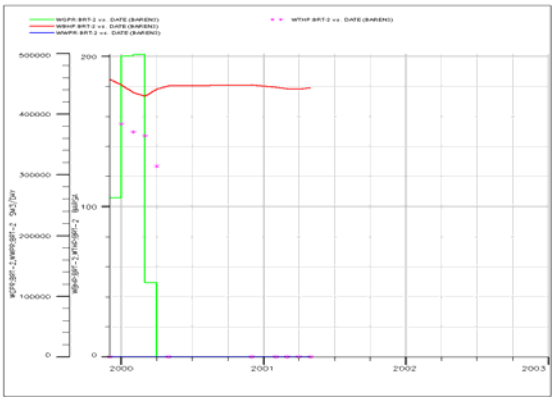

Figure 6b: Gas production, calculated BHP and THP of well BRT-2.

3.2 Predictions

Starting date for the prediction runs was January 1, 2002, the assumed closure of the Barendrecht field. The simulation period was at least 25 year in correspondence with the expected life time of the Barendrecht thermal project. The required minimum economical production rate was 100 m^{3}/hr and an injection temperature of 50 ^{o}C.

The location of the production well was chosen to achieve a high production water temperature and a low pressure decline in the reservoir. Favourable large sand bodies at relative large depth can be found in a northeasterly direction. The optimal distance between production and injection well can be calculated analytically (Muskat, 1937) for a homogeneous reservoir with constant permeability and porosity. This distance is 1000 – 2000 m for the production rate of 100 m^{3}/hr.

A location of the production well (BRT-3) in northeasterly direction was selected at a distance of 1800 m with respect to the injection well (BRT-1). The temperature change (Figure 7) and pressure change (Figure 8) in time in the wells according to the numerical model are small.

The temperature distribution in the reservoir after 25 year of operation is shown in Figure 9.

The injected water does not enter the production well. The largest pressure differences of course are found close too the wells. To the boundaries of the model the pressure differences with respect to the initial pressure are very small.

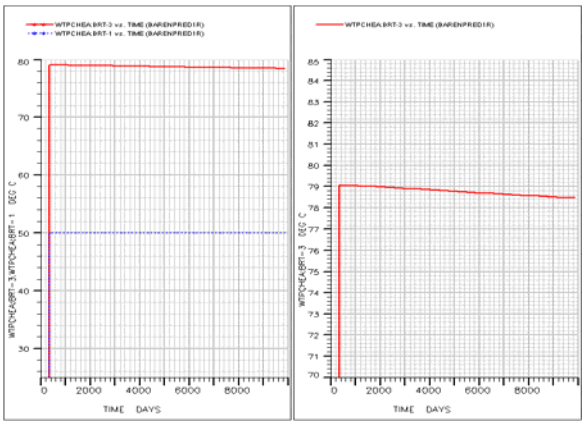

Figure 7: The temperature variation in time in the injection well BRT-1 and the production well BRT-3.

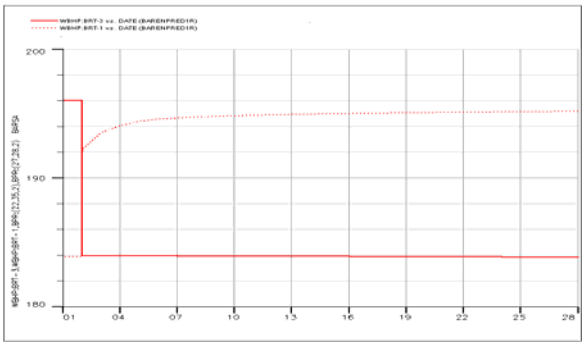

Figure 8: The pressure in the wells BRT-1 (injection well) and BRT-3 (production well).

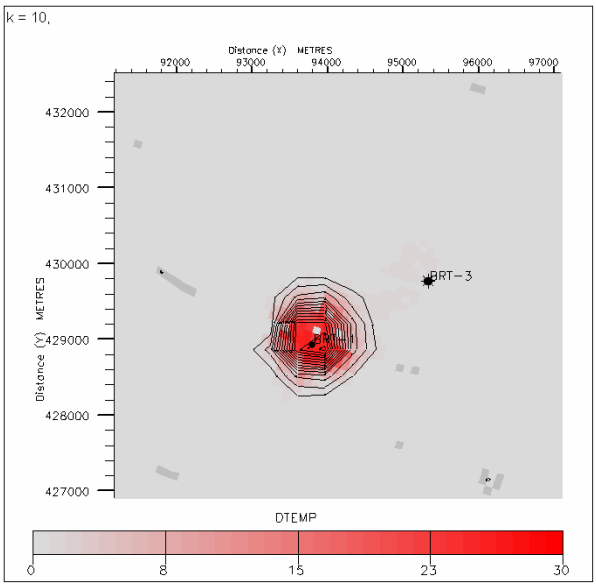

Figure 9: The difference in temperature after 25 year of operation.

Vertical temperature disturbance

With a standard Eclipse model the heat transport below and above the reservoir can not be estimated. However there is heat transport through impervious layers. For this reason three layers with an individual thickness of 100 m above and below the reservoir have been added to the model. The temperature difference after 25 years of production is again small and less than 0.5 ^{o}C.

4. THE INDUCED STRESSES AND ASSOCIATED DEFORMATION

4.1 Background

The processes of fluid flow and heat flow in a geothermal reservoir change reservoir pressure and temperature. Due to the coupling with the stress, pressure and temperature changes cause stress changes in the subsurface and associated deformation. This section presents an estimate of the magnitude of induced poroelastic and thermoelastic stresses and the resulting reservoir deformation, caused by production and injection of water into the geothermal reservoir under consideration.

4.1.1 Poroelastic stress

The upper bound of poroelastic and thermoelastic stress due to production in geothermal reservoirs can be conveniently estimated for the rock which is not constrained by the confining stresses. Hence, the relationships given below can be interpreted as an order-of-magnitude estimate of the upper bound of the induced stresses (Segall and Fitzerald, 1998).

The poroelastic stress can be estimated as follows:

$$\sigma_{ij}^{poro} = -\alpha \, \Delta p \tag{2}$$

$$\alpha = 1 - \gamma = 1 - \frac{K_D}{K_S} \tag{3}$$

where $\sigma_{ij}^{poro}, \alpha, \Delta p, \gamma, K_D, K_S$ are the poroelastic stress, Biot's coefficient (for soil, unconsolidated and weak rock $\alpha = 1$; for hard rock $0.5 < \alpha < 1$), pressure change, compressibility function, compression modulus of the drained porous soil skeleton and compression modulus of the non-porous solid, respectively.

An increase in the pore pressure causes extensional poroelastic stresses and an increase in volume of the porous medium, i.e. dilatation. A decrease in the pore pressure causes compressive poroelastic stresses and compaction.

4.1.2 Thermoelastic stress

The thermoelastic stress can be estimated as follows:

$$\sigma_{ij}^{thermo} = K \, \lambda \, \Delta T \tag{4}$$

$$K = \frac{E}{3(1-2\nu)} \tag{5}$$

where $\sigma_{ij}^{thermo}, K, E, \nu, \lambda, \Delta T$ are the thermoelastic stress, bulk modulus (defined as the ratio of hydrostatic pressure to the relative volume change),Young's modulus, Poisson's coefficient, coefficient of linear thermal expansion and change in temperature, respectively.

An increase in temperature causes an increase in volume, i.e. thermal expansion, and occurrence of extensional thermoelastic stresses. A decrease in temperature causes a reduction in volume and compressional stresses.

The coefficient of linear thermal expansion λ is defined as the ratio of the change of length per degree C to the length

at 0°C. The coefficient of volume expansion λ_v is approximately 3 times the linear expansion coefficient, $\lambda_v = 3\,\lambda$.

4.1.3 Relation between poro- and thermoelasticity

Thermal expansion or contraction and expansion or contraction due to variations in pore pressure have a similar effect on the bulk stress-strain system. The transformation between the two cases is given by the following relation (Geertsma, 1966):

$$\alpha\,\Delta p \leftrightarrow 3\,\lambda\,K\,\Delta T \tag{6}$$

By using this relation it is possible to predict deformation due to thermal effects by using the same approach as when predicting deformation due to poroelastic effects.

4.1.4 Deformation due to poro- and thermoelastic stress

In reservoir geomechanics, the elastic compaction of a depleting reservoir is usually calculated using the model of uniaxial compaction, i.e. in conditions without lateral deformation (Fjær et al., 1992):

$$\Delta h = h\,C_m\,\Delta p \tag{7}$$

where $\Delta h, h, C_m, \Delta p$ are the reservoir compaction, reservoir thickness, coefficient of uniaxial compaction and change in reservoir pressure, respectively.

The coefficient of uniaxial compaction C_m relates the vertical strain $\Delta h / h$ to the pressure drop Δp in uniaxial conditions. It can be calculated from the previously defined elastic parameters:

$$C_m = \frac{\Delta h}{h}\frac{1}{\Delta p} = \frac{1+\nu}{1-\nu}\frac{1-2\nu}{E} \tag{8}$$

The relation given in Equation 6 enables the use of Equation 7 for predicting the elastic compaction due to thermal effects in a geothermal reservoir.

4.2 Elastic and thermal properties of the IJsellmonde sandstone

Equations 2 through 5 show that the thermoelastic stresses depend on both elastic and thermal properties of the porous medium. The bulk modulus *K* can be calculated from Equation 5 for estimated ranges of the elasticity modulus *E* and the Poisson's ratio ν for the IJsselmonde Sandstone. At this stage of the project the site-specific data were not available and we used literature data to derive *K*. The compilation presented in Table 3 is, however, not based on the data obtained in the Netherlands, but on the properties of sandstone measured world-wide, which have been reported in textbooks and manuals of physical constants (Lizenberg et al., 1987).

In order to decrease the uncertainty ranges for elasticity modulus given in Table 1, we use data from previous geomechanical modelling studies of Dutch gas fields (Roest and Kuilman, 1993; Roest et al., 1998). These studies report the measured values of elasticity modulus for the reservoir rock and give an estimate of the elasticity moduli for the overburden, including the Rijnland Formation. The elasticity modulus of the Rijnland Formation (and the IJsselmonde Sandstone) will be lower than E < 30 GPa, possibly E = 10-20 GPa. The Poisson's coefficient could well be in the range ν = 0.15-0.20. Introducing the values of E=10-20 GPa and ν = 0.15-0.20 in Equation 5, we obtain the bulk modulus in the range of K = 5-10 GPa. Introducing the same values for E and ν in Equation 8, we obtain the coefficient of uniaxial compression in the range of Cm=1x10^{-4} – 5x10^{-5} MPa^{-1}.

Table 3: Thermomechanical properties of sandstone and greywake (based on a Thermo-Mechanical Data Base compiled by Lizenberg et al., 1987).

Elasticity modulus of sandstone and greywake, E [GPa]	Shaly	10 ± 7
	Normal	30 ± 10
	Quartzitic	60 ± 10
Poisson's coefficient, ν [-]		0.15 ± 0.1
Coefficient of linear thermal expansion, λ [10^{-5} ºK^{-1}]		1 ± 0.2

For determination of the thermal properties of the sandstone, we also rely on literature data. The coefficient of linear thermal expansion is generally dependent on the mineralogy of the sandstone. Thermal properties for some mineral phases have been measured and are given in Table 4 (Hosni et al., 2003).

Table 4: Thermomechanical properties of some mineral phases (Hosni et al., 2003).

Mineral type	K - Feldspars	Altered Plagio-clases	Quartz	Black minerals, mainly Biotite
Coefficient of linear thermal expansion, λ [10^{-5} ºC^{-1}]	0.385	1.4	3.5	1.4

A typical value for the coefficient of linear thermal expansion, reported in a number of papers related to the modelling of test sites for geological disposal of radioactive waste, is λ=1x10^{-5} C^{-1} (Stephansson et al., 2003). In further calculations we adopted this value and a value of $\lambda_v = 3x10^{-5}\ ^{\circ}C^{-1}$ for the coefficient of volumetric thermal expansion.

4.3 Estimation of poroelastic stress and related deformation for Barendrecht

Equation 2 shows that the poroelastic stresses are proportional to a change in the pore pressure in a geothermal reservoir, assuming that $\alpha = 1$, which is valid if the non-porous solid is incompressible. This assumptions yields the maximal poroelastic stresses, as $\alpha \le 1$.

Due to a high permeability of the IJsselmonde Sandstone (k = 1000 mD) and supposedly its high injectivity, it may be assumed that the cold water will be injected at a low over-pressure into a geothermal reservoir. Previous modelling has shown that the over-pressure will not exceed 10 bars

(Geothermal Project Carnisselande, 2001). In this case the induced poroelastic stresses will be in the order of 1 MPa, i.e. $\sigma_{ij}^{poro} = 1\,MPa$. In the depleting part of the reservoir, which is spread around the producing well, the poroelastic stresses are compressive and cause reservoir compaction. The total compaction of the 40-m thick IJsselmonde Sandstone due to the compressive poroelastic stresses of 1 MPa, according to Equation 7, amounts to:

$$\Delta h = 40\,m\,(1x10^{-4} - 5x10^{-5}\ MPa^{-1})\,1\,MPa = 2 - 4\,mm$$

In the part of the reservoir around the injection well, where the pore pressure has increased with reference to the virgin pressure, the poroelastic stresses are extensional and cause dilatation of the sandstone and rebound, i.e. uplift. According to the theory of elasticity, the rebound caused by water injection at an over-pressure of 1 MPa will be equal to the subsidence caused by a pressure decline of 1 MPa. In reality, the rebound is likely to be a fraction of subsidence.

4.4 Estimation of thermoelastic stress and related deformation for Barendrecht

The thermoelastic stresses can be estimated from Equation 4 by assuming that *K=5-10 GPa* and $\lambda = 1x10^{-5}\ C^{-1}$. We obtain $\sigma_{ij}^{thermo} = 0.05 - 0.1\,MPa/^{\circ}C$. For $\Delta T = 50\ ^{\circ}C$, the thermal stresses amount to $\sigma_{ij}^{thermo} = 2.5 - 5\,MPa$. This can be regarded as the upper bound of the thermal stresses in the geothermal reservoir. The upper bound of thermal compressive stresses due to cooling is significantly higher than that obtained for poroelastic stresses.

The total compaction due to the injection of cold water into the geothermal reservoir can be estimated from Equation 7 using the transformation given in Equation 6:

$$\Delta h = h\,C_m\,\lambda_v\,K\,\Delta T \qquad (9)$$

$$\Delta h = 40\,m\,(1x10^{-4} - 5x10^{-5}\ MPa^{-1})\,3x10^{-5}\,^{\circ}C^{-1}\,(5-10)x10^{3}\ MPa$$

$$\Delta h = 6x10^{-4}\ m/^{\circ}C$$

For a temperature drop of $\Delta T = 50\ ^{\circ}C$ we obtain the total compaction of $\Delta h = 3\,cm$.

Additional stresses may be induced in the geothermal reservoir, as a result of heating/cooling of the pore water and subsequent change in the pore pressure. The coefficient of thermal expansion of water is much larger than the coefficient of the rock solid (in our case 25 to 60 times, Table 5; the literature suggests 100 times larger values). This effect becomes significant for porous media of low permeability (k<10 mD or even more for k<1 mD). For the IJselmonde Sandstone of high permeability this effect is insignificant.

Table 5: Properties of pure water (Matthess, 1982).

Tempe-rature, [°C]	Density, ρ [g/cm^3]	Dynamic viscosity, μ [10^{-3}Pa s]	Coefficient of cubic thermal expansion, for pressure range of 15-20 MPa, λ_v [10^{-5} °C^{-1}]
20	0.99820	1.0050	25
70	0.97778	0.4061	60

4.5 Superposition of poro- and thermoelastic effects

In the part of the reservoir around the injection well, the poroelastic effects due to over-pressurising will yield extensional stresses, which will partly reduce the thermoelastic compressional stresses due to cooling. In the close vicinity of the injection well, where the upper bounds apply, the thermoelastic stresses of 2.5-5 MPa will be reduced by 1 MPa.

In the depleting part of the reservoir, which extends around the producing well, the thermal effects diminish with the distance from far field towards the producing well, where they are negligible. The opposite is true for the poroelastic stresses. In the close vicinity of the production well, where the upper bounds apply, the thermoelastic stresses are 0 and the compressional poroelastic stresses are about 1 MPa.

4.6 Estimation of poroelastic stress and related deformation by finite element modelling

The poroelastic effects caused by water production from a geothermal reservoir are similar to the poroelastic effects caused by gas extraction from a depleting reservoir. The effects of the same magnitude, but the opposite sign, are caused by water injection, assuming linear elastic conditions.

We will use a geomechanical FE model of the gas reservoir to get an insight into the distribution of stresses and deformation in and around a producing reservoir, or a producing well, for the case of the Barendrecht project.

The finite element model shown in Figure 10, represents a gas field with a similar geometric setting as the Barendrecht geothermal field.

Due to the assumed symmetry of the reservoir, only one half of the reservoir was modelled. The model was developed as a 2D plane strain model with 8-node quadrilateral plane strain elements. The same elastic properties were assumed for the reservoir and the surrounding rock (E=10 GPa, ν=0.2) and a unit pressure drop in the reservoir was applied (1 MPa). The obtained results can be conveniently visualised, as the amount of change in stress is given in fractions of 1.

The most pronounced stress changes are in the reservoir rock (Figures 11 and 12). In the surrounding rock the stress changes are much lower, in the order of a few percents of the change in pore pressure in the reservoir (Δp). Exception is the surrounding rock in the vicinity of the lateral edges of the reservoir, where the stress concentrations occur. The change in vertical stress is practically equal to the change in pore pressure in the reservoir (the factor is close to 1 in Figure 11), while the change in horizontal stress is about one half of *Δp* due to the effect of elastic coupling between the reservoir and the surrounding rock in lateral directions (Figure 12).

As the stress is a tensor quantity, it is convenient to transform it to the equivalent Von Mises stress, which is a scalar quantity, for easier visualisation. The equivalent Von Mises stress σ_{eq} is defined as follows:

$$\sigma_{eq} = \frac{1}{\sqrt{2}}\sqrt{(\sigma_1 - \sigma_2)^2 + (\sigma_2 - \sigma_3)^2 + (\sigma_3 - \sigma_1)^2} \qquad (10)$$

where $\sigma_1, \sigma_2, \sigma_3$ are the three principal stress components.

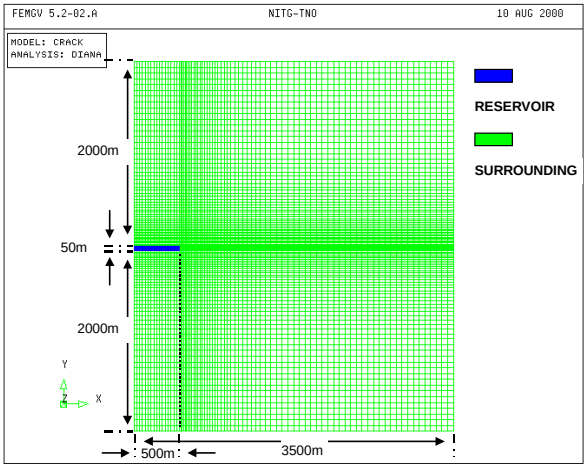

Figure 10: Finite element model of a gas reservoir.

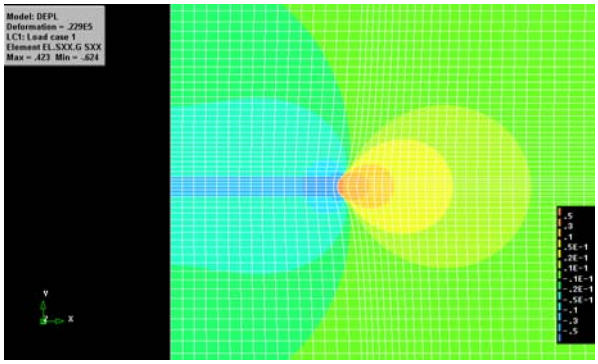

Figure 11: Changes in the vertical stresses in the vicinity of the reservoir due to reservoir depletion. The stresses in the reservoir coloured dark blue will increase by Δp, while the stresses above the reservoir coloured yellow will increase by 2% of Δp.

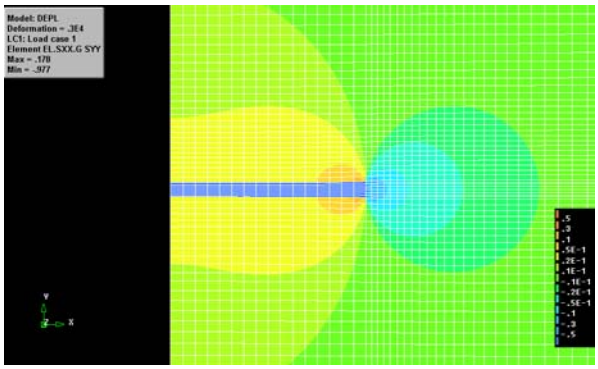

Figure 12: Changes in the horizontal stresses in the vicinity of the reservoir due to reservoir depletion.

The plot of the equivalent stresses in Figure 13 shows the changes in stress localised around the reservoir.

Deformation caused by reservoir depletion is the largest in the compacting reservoir (Figure 14). Deformation propagates from the reservoir to the ground surface more freely, due to unconstrained ground surface, than in other constrained directions. Below the reservoir level, some uplift occurs.

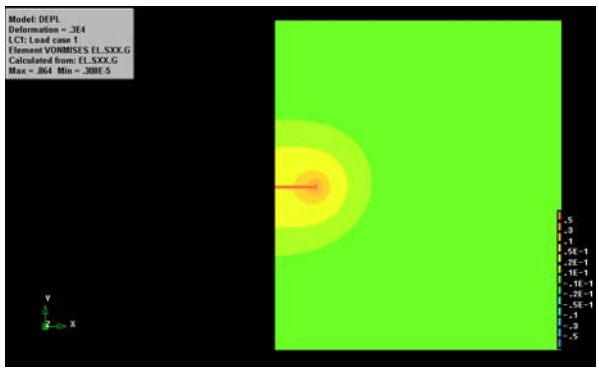

Figure 13: Change in the Von Mises equivalent stresses due to reservoir depletion.

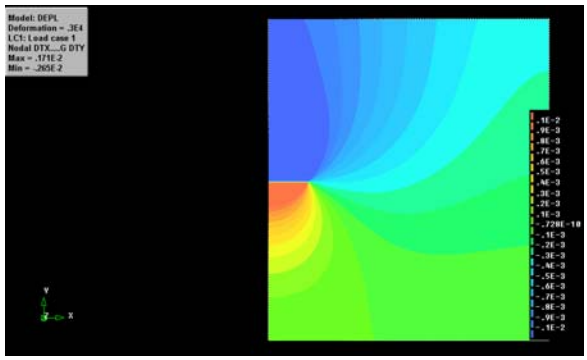

Figure 14: Vertical deformation due to reservoir depletion in the form of subsidence, above the reservoir, and uplift, below the reservoir.

5. CONCLUSIONS

No thermal break through occurs in the lifetime of 25 years of the production system

Far field, or regional, thermal and poroelastic effects on ground deformation are very likely insignificant for a period of 25 years, but may well be significant for a period of 125 years. The latter case likely justifies a modelling study to assess the induced thermo-poro-mechanical effects

Near field coupled thermal, poroelastic and mechanical processes may be significant for borehole stability as the largest thermal stresses due to injection of cold water and transfer of heat occur in the vicinity of the injection well. A modelling study is recommended.

ACKNOWLEDGEMENTS

The Nederlandse Aardolie Maatschappij (NAM) and TNO-NITG carried out a geothermal feasibility study on the mature Barendrecht gas field with the aim to investigate the scope of a geothermal project. This paper reports on technical studies, especially in the area of induced stresses and associated deformations (Section 4). We thank the Nederlandse Aardolie Maatschappij for allowing publication of this paper and in particular the NAM staff that worked on the project: Joost Ketting, Joost van der Burgh, Richard Hakvoort, Jacco Kokkedee and Jonathan Nwaroh. We like also to thank the assistance of Kees Geel and Jo Ramaekers from TNO-NITG.

REFERENCES

De Vault, B., and Jeremiah, J.: Tectonostratigraphy of the Nieuwerkerk Formation (Delfland subgroup), West Netherlands Basin. *AAPG Bulletin*, **86**, (2002), 1679-1707.

Eclipse manual: Technical Description Schlumberger, Geoquest (1998).

Fjær, E., Holt, R.M., Horsrud, P., Raaen, A.M., and Risnes, R.: *Petroleum Related Rock Mechanics*, Developments in Petroleum Sciences 33, Elsevier, (1992), 338.

Geertsma, J.: Problems of rock mechanics in petroleum production engineering, *Proceedings*, First Congress of the Int. Assoc. of Rock Mechanics, Lisbon, (1966), 585-594.

Hosni, A., Gentlier S., Genter A., Riss J., Billaux D., and Dedecker, F.: Coupled THM modelling of the stimulated fractures in the near well at the Soultz-Sous-Forêts site (France), *Proceedings*, International Conference on Coupled T-H-M-C Processes in Geo-systems: Fundamentals, Modelling, Experiments & Applications, Part 2. Royal Institute of Technology, Stockholm, (2003), 665-670.

Liezenberg, J.L., Spiers C.J., and Peach, C.J.: *A Thermo-Mechanical Data Base for Rock Types expected in and around Permian Evaporite Bodies in the Netherlands*, Work performed in the framework of the Dutch national research program (OPL Program, Phase 1) on disposal of radioactive waste in onshore geological formations, Institute of Earth Sciences, University of Utrecht, (1987).

Matthess, G.: *The Properties of Groundwater*, John Wiley & Sons, Inc., (1982), 406.

Muskat, M.: *The flow of homogeneous fluids through porous media*, International human resources development corporation, Boston, (1937).

Racero-Baena, A., and Drake, S.J.: Structural style and reservoir development in the West Netherlands oil province, *in* H. E. Rondeel, H.E., Batjes, D.A.J., and Nieuwenhuijs, W.H., *Geology of gas and oil under the Netherlands*: Dordrecht, Kluwer Academic Publishers, (1996), 211–228.

Roest, J.P.A., and Kuilman, W.: *Geomechanische analyse van de lichte aardschokken in het Eleveld reservoir*, Subfaculty of Applied Earth Sciences, Delft University of Technology, (1993).

Roest, J.P.A., Mulders F.M.M., and Kuilman, W.: Data-limited geomechanical modelling for investigating induced seismicity mechanisms, *Proceedings*, 9th Int. Congr. on Rock Mech. Paris, France, Balkema, Rotterdam, (1998).

Segall, P., and Fitzerald, S.D.: A note on induced stress changes in hydrocarbon and geothermal reservoirs. *Tectonophysics*, **289**, (1998), 117-128.

Somerton, W.H.: *Thermal properties and temperature-related behavior of rock-fluid systems*, Developments in Petroleum Science, **37**, Elsevier, Amsterdam, (1992).

Stephansson, O., Hudson J.A., and Jing, L.: International Conference on Coupled T-H-M-C Processes in Geo-systems: Fundamentals, Modelling, Experiments & Applications, *Proceedings*, Royal Institute of Technology, Stockholm, (2003).

Weast, R.C. (ed): *Handbook of chemistry and physics*, CRC Press, Cleveland Ohio 44128, (1975).